COMMUN. MATH. SCI.
Vol. 20, No. 3, pp. 747–762


# AN OPTIMAL DESIGN OF RANDOM SURFACES IN SOLAR CELLS VIA MINI-BATCH STOCHASTIC GRADIENT APPROACH*

DAN WANG†, QIANG LI‡, AND JIHONG SHEN§

**Abstract.** A resultful way to increase the absorbing efficiency of solar cells is using random rough textures which can trap the optical light and increase the optical path of photons. In this paper, we consider the design problem for two-layer structure thin-film solar cells to find the optimal interface and bottom. We formulate the design problem as a random PDE constrained optimization problem and employ gradient-based methods for solving the problem numerically. To improve the time efficiency, mini-batch stochastic gradient method is used. Numerical examples are shown to test the efficiency of the proposed algorithm.

**Keywords.** Surface optimal design; stochastic gradient method; solar cells.

**AMS subject classifications.** 65C20; 65K10.

## 1. Introduction

Solar cells convert light energy into electric energy through photoelectric effect. With the increasing energy crisis, solar energy, as one of the clean and renewable energy sources, provides a feasible solution to meet the growing energy needs. One representative solar cell is the thin-film solar cell, which is composed of hydrogenated amorphous silicon and nano-silicon thin films. Compared with traditional crystalline silicon solar cells, thin-film solar cells have smaller thickness, lower production cost and some other unique optical properties. However, due to the thickness of amorphous silicon thin-film solar cells, the absorption of light at larger wavelengths is very low since a large number of photons escape. Generally, the efficiency of thin-film solar cells is quiet low.

There are many ways to increase the efficiency of thin-film solar cells, such as antireflection coatings, fluorescent dyes, dielectric gratings, photonic crystals and plasma nanoparticles [1–5]. Another method to improve the absorption efficiency of the solar cell is using the random nano-structure to capture the light beam [6–10]. The introduction of the random interface can reduce the reflection loss of the incident surface since the light can be reflected back into the cell many times. The random nano-structure increases the optical thickness of the cell without changing the physical thickness of the cell.

In this paper, we formulate the optimal design of random surface textures for both transparent conducting oxide (TCO) layer and absorbing (Si:H) layer as a random PDE constrained problem [11]. The mini-batch stochastic gradient descent method is applied to solve the random optimization problem to obtain the statistical optimal parameters of the optimal random textures. It turns out that the mini-batch stochastic gradient descent method can find the optimal value efficiently [12]. It is demonstrated that new random textures give rises to a significant absorption enhancement.

The rest of the paper is structured as follows. Section 2 presents the mathematical modeling for the optimal design problem. In Section 3, the optimal design problem

*Received: April 21, 2021; Accepted (in revised form): August 29, 2021. Communicated by Gang Bao.

†College of Intelligent Systems Science and Engineering, Harbin Engineering University, Harbin, Heilongjiang, 150001, China (wangdancat@hrbeu.edu.cn).

‡Department of Mathematics and Statistics, Auburn University, Auburn, AL, 36849, USA (qzl0011@auburn.edu).

§Corresponding author. College of Intelligent Systems Science and Engineering, Harbin Engineering University, Harbin, Heilongjiang, 150001, China (shenjihong@hrbeu.edu.cn).

is formulated. Section 4 includes the derivation of the gradient for the cost function and the computational algorithm for the optimal design problem. Several numerical experiments are presented in Section 5 to demonstrate the efficiency of the algorithm.

## 2. Mathematical formulation

The optimal design problem seeks to enhance the absorption efficiency of cells, that is to minimize the reflectivity by energy conservation law. The typical structure of a p-i-n Si:H solar cell is shown in Figure 2.1. Since the index contrast between the glass substrate and the TCO is rather low, for simplicity we don't explicitly consider the glass substrate and assume that the cell consists of two layers only. That is, an absorbing layer (e.g., a-Si:H) sits at the bottom and a transparent conducting oxide (TCO) layer lies on the top. The goal is to optimize the random textures for the TCO layer and Si:H layer. The reflection efficiency associated with the solar cell is related to the scattered field. To define the reflectivity, we formulate the scattered field first.

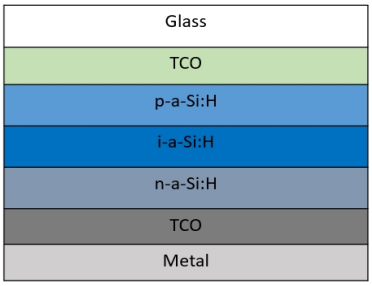


FIG. 2.1. *A typical structure of solar cell.*

**2.1. Optical scattering problem.** In order to facilitate calculation, it is assumed that the whole structure is periodic with the period $\Lambda$ [14,19]. We also assume the cell along the $x_3$ direction is invariant. The solar cell model we consider is the two-dimensional model whose bottom $\Gamma_1$ and interface $\Gamma_2$ are in random manners, as shown in Figure 2.2.

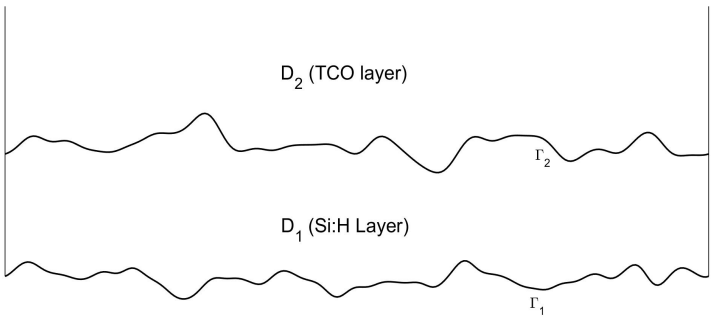


FIG. 2.2. *Schematic plot of the unbounded geometry.*

Let $\Omega$ be the sample space. For a random sample $\omega\in\Omega$, the bottom $\Gamma_1$ and the interface $\Gamma_2$ are denoted as $\Gamma_i(\omega):=\{(x_1,x_2)|x_2=f_i(\omega,x_1)\}$, $i=1,2$, and $\varepsilon_{r,1}$ and $\varepsilon_{r,2}$ are the permittivities in the absorbing layer and TCO layer, respectively. The domains for the absorbing layer and TCO layer are given by:

$$D_1(\omega):=\{(x_1,x_2)|x_1\in(0,\Lambda),f_1(\omega;x_1)<x_2<f_2(\omega;x_1)\}$$
$$D_2(\omega):=\{(x_1,x_2)|x_1\in(0,\Lambda),f_2(\omega;x_1)<x_2<\infty\}.$$

We consider the transverse electric (TE) case for the electric field $E=(0,0,u)$. The random structure is illuminated by an incident time–harmonic plane wave $u^i$ with incident angle $\theta$, $u^i=e^{ik_0q_2d\cdot x}=e^{i(\alpha x_1-\beta x_2)}$, i.e. $\alpha=k_0q_2\sin\theta$, $\beta=k_0q_2\cos\theta$ where $k_0$ is the free-space wavenumber, $q_2:=\sqrt{\varepsilon_{r,2}}$ is the refractive index of the TCO layer and $d=\langle\sin\theta,-\cos\theta\rangle$ is the propagation direction. The total field $u$ after the scattering consists of the incident wave $u^i$ and the scattered wave $u^s$.

In order to formulate the scattering problem in a bounded domain, let us introduce the Dirichlet-to-Neumann map on the line $x_2=b$, where $b>\max\limits_{0<x_1<\Lambda}f_2(\omega;x_1)$. For a fixed sample $\omega$, by virtue of the well-known Rayleigh expansion, the scattered field above $\Gamma_2(\omega)$ can be expressed as

$$u^s(\omega;\cdot)=\sum_{n=-\infty}^{\infty}\hat{u}_n^s(\omega;b)\,e^{i\alpha_nx_1+i\eta_n(x_2-b)},\tag{2.1}$$

where $\hat{u}_n^s(\omega;b)$ are the Fourier coefficients of $u^s(\omega;x_1,b)$, $\alpha_n:=\alpha+\dfrac{2\pi n}{\Lambda}$ for $n\in\mathbb{Z}$ and

$$\eta_n=\begin{cases}\sqrt{k_0^2\varepsilon_{r,2}-\alpha_n^2}, & k>\alpha_n,\\ i\sqrt{\alpha_n^2-k_0^2\varepsilon_{r,2}}, & k<\alpha_n,\end{cases}\tag{2.2}$$

where $k=k_0q_2$. It then follows that for $x_2=b$,

$$\frac{\partial u^s}{\partial x_2}(\omega;x_1,b)=\sum_{n=-\infty}^{\infty}i\eta_n\hat{u}_n^s(\omega;b)e^{i\alpha_nx_1}=:T[u^s(\omega;x_1,b)].\tag{2.3}$$

By noting that $u=u^i+u^s$ and following a direct calculation, we obtain

$$\frac{\partial u}{\partial x_2}(\omega;x_1,b)=T(u(\omega;x_1,b))+g(x_1),$$

where $g(x_1)=-2i\beta e^{i\alpha x_1-i\beta b}$.

We define $\Gamma(\omega):=\Gamma_1(\omega)\cup\Gamma_2(\omega)$ as the union of the random interface and bottom boundary. With the help of the Dirichlet-to-Neumann map on the line $x_2=b>\max f_2$, for each sample $\omega$, the scattering field $u\in L^2(D)$ satisfies the following boundary value problem in the bounded domain shown in Figure 2.3. We denote $D:=\{(x_1,x_2)|0<x_1<\Lambda,f_1(\omega;x_1)\le x_2<b\}$ and assume $f_i\in L^2(0,\Lambda)$, $i=1,2$.

$$\begin{cases}\Delta u(\omega;\cdot)+k_0^2\varepsilon_ru(\omega;\cdot)=0, & \text{in } D\backslash\Gamma(\omega),\\ u(\omega;\Lambda,x_2)=e^{i\alpha\Lambda}u(\omega;0,x_2), & f_1(\omega;0)<x_2<b,\\ u(\omega;x_1,f_1(\omega;x_1))=0, & 0<x_1<\Lambda,\\ \dfrac{\partial u}{\partial x_2}(\omega;x_1,b)=T(u(\omega;x_1,b))+g(x_1), & 0<x_1<\Lambda,\\ u_+(\omega;x_1,f_2(\omega;x_1))=u_-(\omega;x_1,f_2(\omega;x_1)), & 0<x_1<\Lambda,\\ \partial_\nu u_+(\omega;x_1,f_2(\omega;x_1))=\partial_\nu u_-(\omega;x_1,f_2(\omega;x_1)), & 0<x_1<\Lambda,\end{cases}\tag{2.4}$$

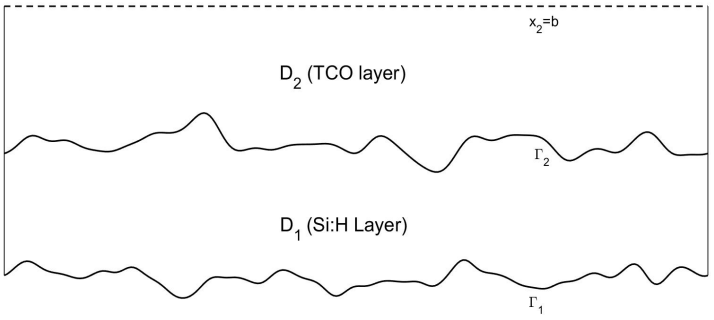


FIG. 2.3. *Schematic plot of the bounded geometry.*

where $\nu$ denotes the unit normal vector along $\Gamma_2(\omega)$ pointing toward $D_2(\omega)$, $u_\pm$ and $\partial_\nu u_\pm$ denote the limits of $u$ and $\partial_\nu u$ from above and below the surface respectively, and $\varepsilon_r = \varepsilon_{r,i},\ (x_1,x_2) \in D_i,\ i=1,2$.

**2.2. Random surface representation.** We assume that the random surface $\Gamma(\omega) := \{(x_1,x_2) | x_2 = f(\omega;x_1)\}$ is a random perturbation of the reference surface with the height $x_2 = f^a$ in the sense that,

$$f(\omega,x_1) = f^a + h(\omega;x_1),$$

where the deviation of the reference surface $h(\omega;x_1)$ is a stationary Gaussian process with zero mean and a continuous and bounded Gaussian-type covariance function. Consider a covariance function defined by inverse exponentiated squared Euclidean distance for the modeling of the rough surface, given by

$$C(x,x') = \sigma^2 exp(-\frac{|x-x'|^2}{\ell^2}),$$

where $\sigma$ is the root mean square (RMS) height of the surface and $\ell$ is the correlation length.

Since $h(\omega;x_1)$ is a centered mean-square continuous stochastic random process, we can represent the texture surface $h(\omega;x_1)$ using Karhunen–Loève expansion [13]. We denote $c(|x-x'|) = C(x,x')$. Since $c(x_1)$ is even, it follows that

$$c(x_1) = \sigma^2 \left[ \frac{\hat{c}_0}{2} + \sum_{p=1}^{\infty} \hat{c}_p \cos\left( \frac{2p\pi x_1}{\Lambda} \right) \right],$$

where $\hat{c}_0,\ \hat{c}_1,\ \hat{c}_2,\ \cdots$ are the Fourier cosine expansion coefficients of the correlation function $c(x_1)$. It can be shown explicitly that the covariance operator $K\varphi(x_1) := \int_0^\Lambda c(x_1-y_1)\,\varphi(y_1)dy_1$, possesses the eigenvalues

$$\lambda_j = \frac{\sigma^2 \Lambda \hat{c}_j}{2}, \quad j = 0,1,2,\cdots,$$

and the corresponding eigenfunctions are

$$\varphi_j(x_1)=\begin{cases}\sqrt{\dfrac{1}{\Lambda}}, & j=0,\\ \sqrt{\dfrac{2}{\Lambda}}\cos\left(\dfrac{2j\pi x_1}{\Lambda}\right), & j>1,\text{even},\\ \sqrt{\dfrac{2}{\Lambda}}\sin\left(\dfrac{2j\pi x_1}{\Lambda}\right), & j>1,\text{odd}.\end{cases}$$

The Karhunen–Loève representation of the random process $h(\omega;x_1)$ is given by

$$h(\omega;x_1)=\sqrt{\lambda_0}\xi_0(\omega)\sqrt{\frac{1}{\Lambda}} +\sum_{j=1}^{\infty}\sqrt{\lambda_j}\left[\xi_{j,s}(\omega)\sqrt{\frac{2}{\Lambda}}\sin\left(\frac{2j\pi x_1}{\Lambda}\right)+\xi_{j,c}(\omega)\sqrt{\frac{2}{\Lambda}}\cos\left(\frac{2j\pi x_1}{\Lambda}\right)\right], \tag{2.5}$$

where $\xi_0$, $\xi_{j,c}$ and $\xi_{j,s}$ are *i.i.d.* Gaussian random variables with zero mean and unit covariance.

Alternatively, by letting $\lambda_j=\sigma^2\bar{\lambda}_j, \bar{\lambda}_j=\dfrac{\Lambda\hat{c}_j}{2}$, we may express the profile of the random surface by

$$h(\omega;x_1)=\sigma\cdot\bar{h}(\omega;x_1), \tag{2.6}$$

where

$$\bar{h}(\omega;x_1)=\sqrt{\bar{\lambda}_0}\xi_0(\omega)\sqrt{\frac{1}{\Lambda}} +\sum_{j=1}^{\infty}\sqrt{\bar{\lambda}_j}\left[\xi_{j,s}(\omega)\sqrt{\frac{2}{\Lambda}}\sin\left(\frac{2j\pi x_1}{\Lambda}\right)+\xi_{j,c}(\omega)\sqrt{\frac{2}{\Lambda}}\cos\left(\frac{2j\pi x_1}{\Lambda}\right)\right].$$

Therefore we can represent $\Gamma_i,\ i=1,2$ as

$$\Gamma_i(\omega_i;\sigma_i,\ell_i):=\{(x_1,x_2)\,|\,x_2=f_i^a+\sigma_i\cdot\bar{h}_i(\omega_i;x_1)\},$$

where $\sigma_i$, $\ell_i$ are the corresponding RMS and correlation length.

## 3. Optimal design of random rough surface

**3.1. Optimal design problem.** From the conservation of energy, it is clear that for each sample $\omega$, we have,

$$R(\omega)+A(\omega)=1,$$

where $R(\omega)$ and $A(\omega)$ are the reflectivity in $D_2$ and the absorptance in $D_1$, respectively. The optimal design problem seeks to lower the reflection efficiency. For each sample $\omega$, the reflection efficiency is defined by

$$R(\omega;f_1,f_2)=\sum_{n\in\mathcal{N}}\frac{\eta_n}{\eta_0}|r_n(\omega)|^2,$$

where $\mathcal{N} := \{n \in \mathbb{Z} \,|\, k_0^2 \varepsilon_{r,2} - \alpha_n^2 > 0\}$ is the set of indices for all propagating modes in the Rayleigh expansion. We adopt the Rayleigh expansion to rewrite the scattered field as

$$u^s(\omega;\cdot) = \sum_{n=-\infty}^{\infty} r_n(\omega) e^{i\alpha_n x_1 + i\eta_n x_2},$$

where $r_n(\omega) = \hat{u}_n^s(\omega;b)e^{-i\eta_n b}$ are the scattered field coefficients, $\hat{u}_n^s$ are the Fourier coefficients of $u^s$. By calculation, it follows that

$$r_n(\omega) = \begin{cases} \hat{u}_n(\omega;b)e^{-i\eta_n b}, & n \neq 0, \\ \hat{u}_n(\omega;b)e^{-i\beta b} - e^{-2ikb}, & n = 0, \end{cases} \tag{3.1}$$

where $\hat{u}_n(\omega;\cdot)$ are the Fourier coefficients of $u(\omega;\cdot)$.

Denote $\alpha = (\alpha_1, \alpha_2), \alpha_i = (\sigma_i, \ell_i)$, $i = 1,2$ where $\sigma_i$ is the root mean square (RMS) height of the surface and $\ell_i$ is the correlation length corresponding to $\Gamma_i$. We define the cost function

$$J(\alpha_1, \alpha_2) := E[R(\omega; f_1, f_2)],$$
$$E[R] := \int_\Omega \sum_{n \in \mathcal{N}} \frac{\eta_n}{\eta_0} |r_n(\omega)|^2 \, dP(\omega).$$

Recall that $\Omega$ and $P$ denote the random sample space and the probability measure, respectively. Then the optimal design problem is to minimize the mean reflectivity $J(\alpha_1, \alpha_2)$, or equivalently, to solve the optimization problem on a suitable region $U_{\alpha_i} \in \mathbb{R}^2$

$$\min_{\alpha_i \in U_{\alpha_i} i=1,2} J(\alpha_1, \alpha_2). \tag{3.2}$$

## 4. Derivation of the gradient

THEOREM 4.1. *For a given sample $\omega$, the gradient $\nabla_\alpha R = [\partial_{\alpha_1} R, \partial_{\alpha_2} R]^\mathsf{T}$ can be expressed as*

$$\partial_{\alpha_1} R = \frac{2}{\Lambda} \sum_{n \in \mathcal{N}} \frac{\eta_n}{\eta_0} Re \left[ (\hat{u}_n(\omega;b) - a_n e^{-2ikb + i\beta b}) \cdot \int_0^\Lambda ([0, \nabla_{\alpha_1} f_1(x_1)]^T \cdot \nu) [\overline{\frac{\partial u}{\partial \nu}} \cdot \frac{\partial u_n^*}{\partial \nu}] dx_1 \right], \tag{4.1}$$

$$\partial_{\alpha_2} R = \frac{2k_0^2}{\Lambda} \sum_{n \in \mathcal{N}} \frac{\eta_n}{\eta_0} Re \left[ (\hat{u}_n(\omega;b) - a_n e^{-2ikb + i\beta b}) \cdot \overline{(\varepsilon_{r,1} - \varepsilon_{r,2})} \cdot \int_0^\Lambda [\bar{u} u_n^*]|_{(x_1, f_2)} \cdot \nabla_{\alpha_2} f_2 dx_1 \right], \tag{4.2}$$

*where $a_0 = 1$ and $a_n = 0$ if $n \neq 0$. $u$ is the solution to the forward problem (2.4), and $u_n^*$ solves the adjoint problem*

$$\begin{cases} \Delta u_n^*(\omega;\cdot) + k_0^2 \bar{\varepsilon_r} u_n^*(\omega;\cdot) = 0, & \text{in } D \setminus \Gamma(\omega), \\ u_n^*(\omega;0,x_2) = e^{i\alpha\Lambda} u_n^*(\omega;\Lambda,x_2), & \\ u_n^*(\omega;x_1, f_1(x_1)) = 0, & 0 < x_1 < \Lambda, \\ \partial_{x_2} u_n^*(\omega;x_1,b) = T^*(u(\omega;x_1,b)) + e^{i\alpha_n x_1}, & \\ (u_n^*)_+(\omega;\cdot) = (u_n^*)_-(\omega;\cdot), & \text{on } \Gamma_2, \\ \partial_\nu (u_n^*)_+(\omega;\cdot) = \partial_\nu (u_n^*)_-(\omega;\cdot), & \text{on } \Gamma_2, \end{cases} \tag{4.3}$$

and $[u_n^* \bar{u}]|_{(x_1,f_2)}$ is the value of $u_n^* \bar{u}$ on the surface $\Gamma_2(\omega)$, $T^*$ is the adjoint operator of $T$ satisfying that $\langle Tu, v\rangle = \langle u, T^* v\rangle$, $\langle \cdot, \cdot \rangle$ stands for the inner product over the function space $L^2(0,\Lambda)$.

**4.1. Proof of Equation (4.1).**

*Proof.* In order to prove Equation (4.1), consider the perturbed bottom $f_1$, the reflectivity for sample $\omega$ is

$$\begin{aligned} R^{\delta}(\omega;f_1,\cdot) &= \sum_{n\in\mathcal{N}} \frac{\eta_n}{\eta_0}|r_n+\delta r_n|^2 \\ &= \sum_{n\in\mathcal{N}} \frac{\eta_n}{\eta_0}\left\{|r_n|^2+2Re[r_n\overline{\delta r_n}]+|\delta r_n|^2\right\}. \end{aligned}$$

From the definition of (3.1), it follows that $\delta r_n = O(\delta u)$ where $\delta u$ is the perturbation of $u$. Due to the perturbation analysis of the boundary value problem (2.4), we have $\delta u = O(\delta f_1)$. Then it follows that $|\delta r_n|^2 = O((\delta f_1)^2)$. We have

$$R^{\delta}(\omega;f_1,\cdot) = R(\omega;f_1,\cdot)+2\sum_{n\in\mathcal{N}} \frac{\eta_n}{\eta_0} Re[r_n\overline{\delta r_n}]+O((\delta f_1)^2).$$

We denote the perturbation of the reflectivity $\delta R := R^{\delta}-R$ and the perturbation of the scattered field $\delta u$, which is

$$\delta R = 2\sum_{n\in\mathcal{N}} \frac{\eta_n}{\eta_0} Re[r_n\overline{\delta r_n}]+O((\delta f_1)^2). \tag{4.4}$$

For each term $r_n\overline{\delta r_n}$, by virtue of (3.1), it follows that

$$r_n\overline{\delta r_n} = \begin{cases} \hat{u}_n(\omega;b)\cdot\dfrac{1}{\Lambda}\displaystyle\int_0^{\Lambda} e^{i\alpha_n x_1}\,\overline{\delta u(\omega;x_1,b)}\,dx_1, & n\neq 0, \\ \left(\hat{u}_n(\omega;b)-e^{-2ikb+i\beta b}\right)\cdot\dfrac{1}{\Lambda}\displaystyle\int_0^{\Lambda} e^{i\alpha_n x_1}\,\overline{\delta u(\omega;x_1,b)}\,dx_1, & n=0. \end{cases} \tag{4.5}$$

For any continuous vector $V(x)$ defined on $\Gamma_1$ and a small number $\delta$, $\Gamma_1$ is perturbed to be $\Gamma_1^{\delta}$, i.e. $\Gamma_1^{\delta}=\Gamma_1+\delta\cdot V$. The region $D_1$ becomes $D_1^{\delta}$ and denote $D^{\delta}=D_2\cup D_1^{\delta}$ and $\Gamma_{\delta}=\Gamma_1^{\delta}\cup\Gamma_2$. On the new region, the total field $u^{\delta}$ satisfies

$$\begin{cases} \Delta u^{\delta}(\omega;\cdot)+k_0^2\varepsilon_r u^{\delta}(\omega;\cdot)=0, & in\ D^{\delta}\setminus\Gamma^{\delta}(\omega), \\ u^{\delta}(\omega;\Lambda,x_2)=e^{i\alpha\Lambda}u^{\delta}(\omega;0,x_2), & \\ u^{\delta}(\omega;x_1,f_1(x_1))=0, & 0<x_1<\Lambda, \\ \partial_{x_2}u^{\delta}(\omega;x_1,b)=T(u^{\delta}(\omega;x_1,b))+g, & \\ u_+^{\delta}(\omega;\cdot)=u_-^{\delta}(\omega;\cdot), & on\ \Gamma_2, \\ \partial_{\nu}u_+^{\delta}(\omega;\cdot)=\partial_{\nu}u_-^{\delta}(\omega;\cdot), & on\ \Gamma_2. \end{cases} \tag{4.6}$$

Denote $H_0^1(D)=\{u\in H^1(D)|u=0\ on\ \Gamma_1, u(\Lambda,x_2)=e^{i\alpha\Lambda}u(0,x_2)\}$. The bilinear form for Equation (2.4) is

$$a(u,w)=\int_D \nabla u\cdot\nabla\bar{w}-k_0^2\varepsilon_r u\bar{w}dx-\langle Tu,w\rangle.$$

The weak solution for (2.4) is $u$, such that

$$a(u,w)=\langle g,w\rangle, \tag{4.7}$$

for all $w \in H_0^1(D)$.
The weak solution for (4.6) is $a^\delta(u^\delta, w^\delta) = \langle g, w^\delta \rangle$ for all $w^\delta \in H_0^1(D)$, where

$$a^\delta(u^\delta, w^\delta) = \int_{D^\delta} \nabla u^\delta \cdot \nabla \bar{w}^\delta - k_0^2 \varepsilon_r u^\delta \overline{w^\delta} dx - \langle T u^\delta, w^\delta \rangle.$$

By extending the definition of $V(x)$ to the closure of $D_1$, we can define a continuous $C^2$ map $\psi$ from $D_1$ to $D_1^\delta$: $X = \psi(Y) = Y + \delta \cdot V(Y), Y \in D_1$, where $\psi$ is identical on the boundary of $D_1$ (Denote the inverse map of $\psi$ as $\phi(X) : D_1^\delta$ to $D_1$).

Let $\tilde{u}^\delta = u^\delta(\psi(y))$, $\tilde{w}^\delta = w^\delta(\psi(y))$, then $\tilde{u}^\delta$, $\tilde{w}^\delta \in D$, from the direct calculation we have

$$a^\delta(u^\delta, w^\delta) = \int_D \Big[ \sum_{m,n=1}^{2} b_{mn} \frac{\partial \tilde{u}^\delta}{\partial y_m} \frac{\partial \overline{\tilde{w}^\delta}}{\partial y_n} - k_0^2 \varepsilon_r \tilde{u}^\delta \overline{\tilde{w}^\delta} \Big] J dy - \langle T \tilde{u}^\delta, \tilde{w}^\delta \rangle,$$

since $\frac{\partial u^\delta}{\partial x_1} = \sum_{m=1}^{2} \frac{\partial \tilde{u}^\delta}{\partial y_m} \frac{\partial \phi_m}{\partial x_1}$, $\phi = [\phi_1, \phi_2]^T$, $J = det D\psi$, $b_{mn} = \sum_{i=1}^{2} \frac{\partial \phi_m}{\partial x_i} \frac{\partial \phi_n}{\partial x_i}$. Define a new bilinear form

$$\tilde{a}^\delta(\tilde{u}^\delta, w) = \int_D \Big[ \sum_{m,n=1}^{2} b_{mn} \frac{\partial \tilde{u}^\delta}{\partial y_m} \frac{\partial \overline{w}}{\partial y_n} - k_0^2 \varepsilon_r \tilde{u}^\delta \overline{w} \Big] J dy - \langle T \tilde{u}^\delta, w \rangle,$$

for $\tilde{u}^\delta, w \in H_0^1(D)$. Then (4.7) is equivalent to finding $\tilde{u}^\delta \in H_0^1(D)$ such that

$$\tilde{a}(\tilde{u}^\delta, w) = \langle g, w \rangle, \tag{4.8}$$

for all $w \in H_0^1(D)$. From (4.7) and (4.8), it is easily seen that $\tilde{u}^\delta - u$ satisfies

$$a(\tilde{u}^\delta - u, w) = -(\tilde{a}^\delta(\tilde{u}^\delta, w) - a(\tilde{u}^\delta, w)).$$

For the right-hand side,

$$a^\delta(u^\delta, w^\delta) = \int_D \Big[ \sum_{m,n=1}^{2} b_{mn} \frac{\partial \tilde{u}^\delta}{\partial y_m} \frac{\partial \overline{\tilde{w}^\delta}}{\partial y_n} - k_0^2 \varepsilon_r \tilde{u}^\delta \overline{\tilde{w}^\delta} \Big] J dy - \langle T \tilde{u}^\delta, \tilde{w}^\delta \rangle.$$

From direct calculation the Jacobian matrix $J$ can be written as:

$$J = 1 + \delta \nabla \cdot V + O(\delta^2),$$

$$(b_{mn}) J = I - \delta(\tilde{b}_{mn}) + O(\delta^2),$$

where $I$ is the $2 \times 2$ identity matrix and

$$(\tilde{b}_{mn}) = \nabla V + (\nabla V)^T - (\nabla \cdot V) I. \tag{4.9}$$

Therefore we have

$$a(\tilde{u}^\delta - u, w) = \delta \int_D \sum_{m,n=1}^{2} \tilde{b}_{mn} \frac{\partial \tilde{u}^\delta}{\partial y_m} \frac{\partial \overline{w}}{\partial y_n} + k_0^2 \varepsilon_r (\nabla \cdot V) u \overline{w} dy + O(\delta^2).$$

Denote $u' = \lim_{\delta \to 0} \dfrac{\tilde{u}^\delta - u}{\delta}$. Then $u'$ satisfies the following equations on $D$.

$$a(u', w) = \int_D \sum_{m,n=1}^{2} b_{mn} \frac{\partial \tilde{u}^\delta}{\partial y_m} \frac{\partial \overline{w}}{\partial y_n} + k_0^2 \varepsilon_r (\nabla \cdot V) u \overline{w} dy. \tag{4.10}$$

Apply $u=w=0$ on $\Gamma_1$ to get $\int_{\Gamma_1}(V\cdot\nabla\bar{w})\frac{\partial u}{\partial\nu}-(\nabla u\cdot\nabla\bar{w})(V\cdot\nu)ds=0$. We then obtain

$$a(u',w)=\int_D \nabla(V\cdot\nabla u)\cdot\nabla\bar{w}-k_0^2\varepsilon_r(V\cdot\nabla\bar{u})\bar{w}dy \text{ for any } w\in H_0^1(D)\cap H^2(D).$$

Then $u'$ satisfies the following boundary value problem,

$$\begin{cases}\Delta u'(\omega;\cdot)+k_0^2\varepsilon_r\delta u(\omega;\cdot)=(\Delta+k_0^2\varepsilon_r)(V-\nabla u), & \text{in } D\setminus\Gamma(\omega),\\ u'(\omega;0,x_2)=e^{i\alpha\Lambda}u'(\omega;\Lambda,x_2),\\ u'(\omega;x_1,f_1(x_1))=0, & 0<x_1<\Lambda,\\ \partial_{x_2}u'(\omega;x_1,b)=T(u^\delta(\omega;x_1,b)), & 0<x_1<\Lambda.\end{cases}$$

Let $u^0=u'-V\cdot\nabla u$, then $u^0=u'$ on $x_2=b$, and $u^0$ satisfies

$$\begin{cases}\Delta u^0(\omega;\cdot)+k_0^2\varepsilon_r u^0(\omega;\cdot)=0, & \text{in } D_\Lambda^\delta\setminus\Gamma(\omega),\\ u^0(\omega;0,x_2)=e^{i\alpha\Lambda}u^0(\omega;\Lambda,x_2),\\ u^0(\omega;x_1,h(x_1))=-(V\cdot\nu)\frac{\partial u}{\partial\nu}, & 0<x_1<\Lambda,\\ \partial_{x_2}u^0(\omega;x_1,b)=T(u^0(\omega;x_1,b)),\\ u_+^0(\omega;\cdot)=u_-^0(\omega;\cdot), & \text{on } \Gamma_2,\\ \partial_\nu u_+^0(\omega;\cdot)=\partial_\nu u_-^0(\omega;\cdot), & \text{on } \Gamma_2.\end{cases}\tag{4.11}$$

Multiplying the solution $u_n^*(\omega;\cdot)$ of the boundary value problem in the adjoint problem (4.3) by $\overline{u^0(\omega;\cdot)}$ and multiplying $u_n^*(\omega;\cdot)$ by the complex conjugate for solution $u^0(\omega;\cdot)$ of (4.11), then integrating over the domain $D_i, i=1,2$ respectively, it follows that

$$\int_{D_i}(\Delta u_n^*(\omega;\cdot)+k_0^2\overline{\varepsilon_r}u_n^*(\omega;\cdot))\overline{u^0(\omega;\cdot)}-u_n^*(\omega;\cdot)\overline{(\Delta u^0(\omega;\cdot)+k_0^2\varepsilon_r u^0(\omega;\cdot))}\,dx=0,\quad i=1,2.$$

By applying Green's formula and imposing the boundary conditions, we obtain

$$-\int_0^\Lambda(V\cdot\nu)\left[\overline{\frac{\partial u(\omega;\cdot)}{\partial\nu}}\cdot\frac{\partial u_n^*(\omega;\cdot)}{\partial\nu}\right]dx_1+\int_{\Gamma_2}\frac{\partial u_n^*(\omega;\cdot)}{\partial\nu}u^0(\omega;\cdot)-u_n^*(\omega;\cdot)\frac{\partial u^0(\omega;\cdot)}{\partial\nu}ds=0,$$

$$\int_{\Gamma_2}\frac{\partial u_n^*(\omega;\cdot)}{\partial\nu}u^0(\omega;\cdot)-u_n^*(\omega;\cdot)\frac{\partial u^0(\omega;\cdot)}{\partial\nu}ds+\int_0^\Lambda\overline{u^0(\omega;\cdot)}(T^*(u_n^*(\omega;\cdot)+e^{i\alpha_n x_1}))$$
$$-u_n^*(\omega;\cdot)T(u^0(\omega;\cdot))dx_1=0.$$

Adding the above equations together yields

$$\int_0^\Lambda e^{i\alpha_n x_1}\,\overline{u^0(\omega;x_1,b)}\,dx_1=\int_0^\Lambda(V\cdot\nu)\frac{\overline{\partial u}}{\partial\nu}\frac{\partial u_n^*}{\partial\nu}dx_1,$$

since $T^*$ is the adjoint operator of $T$. Due to formula (4.4), we have

$$\delta R=\frac{2}{\Lambda}\sum_{n\in\mathcal{N}}\frac{\eta_n}{\eta_0}Re[(\hat{u}_n(\omega;b)-a_ne^{-2ikb+i\beta b})\cdot\int_0^\Lambda(V\cdot\nu)\left[\frac{\overline{\partial u}}{\partial\nu}\frac{\partial u_n^*}{\partial\nu}\right]dx_1]+O(\delta^2).$$

By choosing $V=[0,\frac{\partial f_1}{\partial\sigma_1}]$, we have

$$\frac{\partial R}{\partial\sigma_1}=\frac{2}{\Lambda}\sum_{n\in\mathcal{N}}\frac{\eta_n}{\eta_0}Re[(\hat{u}_n(\omega;b)-a_ne^{-2ikb+i\beta b})\cdot\int_0^\Lambda([0,\frac{\partial f_1}{\partial\sigma_1}]\cdot\nu)\left[\frac{\overline{\partial u}}{\partial\nu}\frac{\partial u_n^*}{\partial\nu}\right]dx_1].$$

Similarly, choosing $V=[0,\dfrac{\partial f_1}{\partial \ell_1}]$, we have

$$\frac{\partial R}{\partial \ell_1}=\frac{2}{\Lambda}\sum_{n\in\mathcal{N}}\frac{\eta_n}{\eta_0}Re[(\hat{u}_n(\omega;b)-a_n e^{-2ikb+i\beta b})\cdot\int_0^{\Lambda}([0,\frac{\partial f_1}{\partial \ell_1}]\cdot\nu)\left[\frac{\overline{\partial u}}{\partial\nu}\frac{\partial u_n^*}{\partial\nu}\right]dx_1],$$

Therefore,

$$\partial_{\alpha_1}R=\frac{2}{\Lambda}\sum_{n\in\mathcal{N}}\frac{\eta_n}{\eta_0}Re[(\hat{u}_n(\omega;b)-a_n e^{-2ikb+i\beta b})\cdot\int_0^{\Lambda}([0,\nabla_{\alpha_1}f_1(x_1)]^T\cdot\nu)\left[\frac{\overline{\partial u}}{\partial\nu}\frac{\partial u_n^*}{\partial\nu}\right]dx_1].$$

□

**4.2. Proof of equation (4.2).**

*Proof.* To prove (4.2), we first derive the shape derivative $\nabla_{f_2}R$. To this end, one needs to derive the perturbation of the reflectivity $\delta R$ due to the perturbation of the interface by $\delta f_2$. When the interface $\Gamma_2$ is perturbed to be $f_2^\delta:=f_2+\delta f_2$ so that the permittivity in the solar cell becomes $\varepsilon_r^\delta:=\varepsilon_r+\delta\varepsilon_r$. The perturbed reflectivity for sample $\omega$ is

$$\begin{aligned}R^\delta(\omega;\cdot,f_2)&=\sum_{n\in\mathcal{N}}\frac{\eta_n}{\eta_0}|r_n+\delta r_n|^2\\&=\sum_{n\in\mathcal{N}}\frac{\eta_n}{\eta_0}\left\{|r_n|^2+2Re[r_n\overline{\delta r_n}]+|\delta r_n|^2\right\}.\end{aligned}$$

From the definition of (3.1), it follows that $\delta r_n=O(\delta u)$ where $\delta u$ is the perturbation of $u$. Due to the perturbation analysis of the boundary value problem (2.4), we have $\delta u=O(\delta\varepsilon_r)$ and $\delta\varepsilon_r=(\varepsilon_{r,1}-\varepsilon_{r,2})\cdot\delta f_2$. Then it follows that $|\delta r_n|^2=O((\delta f_2)^2)$. We have

$$R^\delta(\omega;\cdot,f_2)=R(\omega;\cdot,f_2)+2\sum_{n\in\mathcal{N}}\frac{\eta_n}{\eta_0}Re[r_n\overline{\delta r_n}]+O((\delta f_2)^2).$$

As a result of perturbation analysis, $\delta u$ satisfies the following equations:

$$\begin{cases}\Delta\delta u(\omega;\cdot)+k_0^2\varepsilon_r\delta u(\omega;\cdot)=-k_0^2\delta\varepsilon_r u(\omega;\cdot), & \text{in } D\backslash\Gamma(\omega),\\ \delta u(\omega;\Lambda,x_2)=e^{i\alpha\Lambda}\delta u(\omega;0,x_2),\\ \delta u(\omega;x_1,f_1(x_1))=0, & 0<x_1<\Lambda,\\ \dfrac{\partial\delta u}{\partial x_2}(\omega;x_1,b)=T(\delta u(\omega;x_1,b)), & 0<x_1<\Lambda,\\ (\delta u)_+(\omega;x_1,f_2(\omega,x_1))=(\delta u)_-(\omega;x_1,f_2(\omega,x_1)), & 0<x_1<\Lambda,\\ (\partial_\nu\delta u)_+(\omega;x_1,f_2(\omega,x_1))=(\partial_\nu\delta u)_-(\omega;x_1,f_2(\omega,x_1)), & 0<x_1<\Lambda.\end{cases}\tag{4.12}$$

By multiplying the PDE in the adjoint problem (4.3) by $\overline{\delta u}$ and the PDE in (4.12) by $\overline{u_n^*}$, and integrating over the domain $D_1$ and $D_2$ respectively, it follows that

$$\int_{D_j}(\Delta u_n^*+k_0^2\overline{\varepsilon_r}u_n^*)\,\overline{\delta u}-u_n^*\,\overline{(\Delta\delta u+k_0^2\varepsilon_r\delta u)}\,dx=\int_{D_j}u_n^*k_0^2\overline{\delta\varepsilon_r u}\,dx,\quad j=1,2.$$

An application of the Green's second identity for the left-hand sides and adding the above two equations together, yields

$$\int_{\Gamma_2(\omega)}(\partial_\nu u_n^*)_-\overline{(\delta u)}_--(u_n^*)_-\overline{(\partial_\nu\delta u)}_-ds+\int_{\Gamma_2(\omega)}(u_n^*)_+\overline{(\partial_\nu\delta u)}_+-(\partial_\nu u_n^*)_+\overline{(\delta u)}_+ds$$

$$+\int_0^\Lambda e^{i\alpha_n x}\,\overline{\delta u(\omega;x_1,b)}\,dx_1 = k_0^2\int_{D_1\cup D_2}\delta\bar{\varepsilon}_r\bar{u}u_n^*\,dx.$$

This can be further reduced to the following from the continuity condition along the interface $\Gamma_2(\omega)$:

$$\int_0^\Lambda e^{i\alpha_n x}\,\overline{\delta u(\omega;x_1,b)}\,dx_1 = k_0^2\int_D \delta\bar{\varepsilon}_r\bar{u}u_n^*\,dx.$$

Consequently, in light of (4.4) and (4.5), the perturbation of the reflectivity is expressed by

$$\delta R = \frac{2k_0^2}{\Lambda}\sum_{n\in\mathcal{N}}\frac{\eta_n}{\eta_0}Re\Big[(\hat{u}_n(\omega;b)-a_ne^{-2ikb+i\beta b})\cdot\int_D\delta\bar{\varepsilon}_r\bar{u}u_n^*\,dx\Big]+O(\delta f_2^2).$$

It is observed that for any test function $v\in L^2(D)$, the inner product

$$(v,\delta\varepsilon_r) := \int_D v(x)\,\overline{\delta\varepsilon_r}(x)\,dx = \int_{\text{symdiff}(D_1,D_1^\delta)} v(x)\,\overline{\delta\varepsilon_r}(x)\,dx.$$

Here $D_1$ and $D_1^\delta$ are the corresponding absorbing layers with the interfaces $f_2$ and $f_2^\delta$, respectively, and the symmetric difference of two sets $D_1$ and $D_1^\delta$ is given by

$$\text{symdiff}(D_1,D_1^\delta) = (D_1\cup D_1^\delta)\backslash(D_1\cap D_1^\delta).$$

Now in view of the fact that the relative permittivity of the absorbing and TCO layers are $\varepsilon_{r,1}$ and $\varepsilon_{r,2}$ respectively, the above inner product can be simplified as

$$(v,\delta\varepsilon_r) = \int_0^\Lambda v(x_1,f_2(x_1))\,\overline{(\varepsilon_{r,1}-\varepsilon_{r,2})}\cdot\delta f_2\,dx, \tag{4.13}$$

for an infinitesimal $\delta f_2$. Then we get

$$\delta R = \frac{2k_0^2}{\Lambda}\sum_{n\in\mathcal{N}}\frac{\eta_n}{\eta_0}Re\Big[(\hat{u}_n(\omega;b)-a_ne^{-2ikb+i\beta b})\cdot\overline{(\varepsilon_{r,1}-\varepsilon_{r,2})}\cdot\int_0^\Lambda[\bar{u}u_n^*]|_{(x_1,f_2)}\cdot\delta f_2 dx_1\Big] + O(\delta f_2^2).$$

The desired formula (4.2) for $\nabla_{\alpha_2}R$ then follows by the chain rule. ∎

**4.3. The stochastic gradient descent method.** We will use gradient-based methods to solve the optimization problem (3.2), the derivation of the gradient is given in the previous section. Stochastic gradient descent (SGD) method [15–17] is a widely used method. In gradient descent (GD) method we need to compute the gradient $\nabla_\alpha J$ in every iteration, however in SGD method we only need to compute the gradient $\nabla_\alpha R$ for the iteration. Although the SGD method can effectively improve the efficiency of the algorithm, due to the small number of sampling, the results of the algorithm have serious oscillations. On the part of optimization calculation, we choose to adopt the mini-batch SGD method to reduce the oscillation. The algorithms for GD, SGD and mini-batch SGD are given as follows.

**Algorithm 1** The algorithm for GD method

Initialize $\alpha$ and choose $N$ large enough

**for** $iteration = 1,2,\ldots$ **do**

  **for** $sample = 1,2,\ldots,N$ **do**

    choose random realization of $\Gamma_1$ and $\Gamma_2$

    solve the boundary value problem (2.4) and adjoint problem (4.3)

    Compute sample gradient $\nabla_\alpha R = \nabla_\alpha R(\omega_i)$

  **end for**

  $\nabla_\alpha J = \frac{1}{N}\sum_{i=1}^{N} \nabla R_\alpha(\omega_i)$

  update $\alpha = \alpha - l * \nabla_\alpha J$, (where $l$ is the step length)

**end for**

Return $\alpha$

**Algorithm 2** The algorithm for SGD method

Initialize $\alpha$

**for** $iteration = 1,2,\ldots$ **do**

  choose random realization of $\Gamma_1$ and $\Gamma_2$

  solve the boundary value problem (2.4) and adjoint problem (4.3)

  Compute sample gradient $\nabla_\alpha R = \nabla_\alpha R(\omega_i)$

  update $\alpha = \alpha - l * \nabla_\alpha R$, (where $l$ is the step length)

**end for**

Return $\alpha$

**Algorithm 3** The algorithm for mini-batch SGD method

Initialize $\alpha$

**for** $iteration = 1,2,\ldots$ **do**

  **for** $sample = 1,2,\ldots,N_m$, ($N_m$ can be much smaller than $N$ **do**)

    choose random realization of $\Gamma_1$ and $\Gamma_2$

    solve the boundary value problem (2.4) and adjoint problem (4.3)

    Compute sample gradient $\nabla_\alpha R = \nabla_\alpha R(\omega_i)$

  **end for**

  $G := \frac{1}{N_m}\sum_{i=1}^{N_m} \nabla R_\alpha(\omega_i)$

  update $\alpha = \alpha - l * G$, (where $l$ is the step length)

**end for**

Return $\alpha$

## 5. Numerical experiments

In this section, we present several numerical examples to demonstrate the efficiency of the numerical algorithms for solving the optimal design problem. Monte-Carlo method is used for sampling the probability space. We stop the iteration steps when the gradient is less than 0.05. The first numerical example tests the efficiency of mini-batch stochastic gradient descent method for solving the optimal problem compared to gradient descent method and stochastic gradient method. In the second example, we show the result for the optimal problem when the incident wave has a larger wavelength in which case the absorptance is much smaller.

In all examples, the height of the reference surface, or equivalently the average thickness of the absorbing layer, is set as $a=300$ nm, and the size of the periodic cell $\Lambda=1500$ nm.

**Example 1.** Consider the optimal design under the normal incidence, that is, the incident angle $\theta=0$. Assume that the free space wavenlength $\lambda_0=650$ nm. The refractive index of the TCO layer is 1.915, or equivalently, its relative permittivity $\varepsilon_{r,1}=3.667$ [7, 9, 10]. The refractive index of the absorbing layer is set as $4.2+0.045i$ when $\lambda_0=650$ nm [18]. This implies that the relative permittivity $\varepsilon_{r,2}=17.6380+0.3780i$. We consider the incident angle case $\theta=0$. The initial condition is chosen to be $\alpha_1=(\sigma_1,\ell_1)=(35nm,20nm)$, $\alpha_2=(\sigma_2,\ell_2)=(35nm,20nm)$. We apply the gradient descent method, stochastic gradient method and mini-batch SGD method to solve the optimization problem (3.2) separately. The results are shown in Figure 5.1 to Figure 5.3. The optimal parameters are listed in Table 5.1.

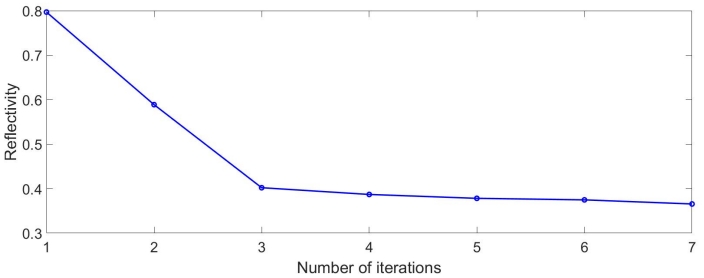


FIG. 5.1. *The cost function $J(\alpha)$ for all iterations using gradient descent method.*

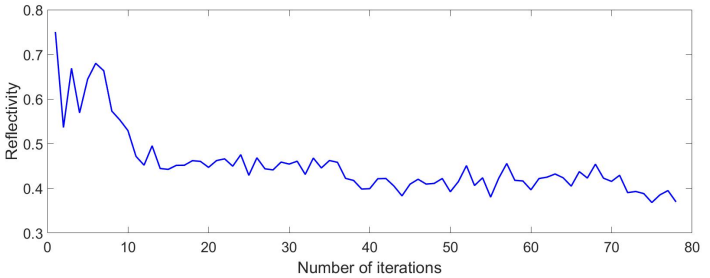


FIG. 5.2. *The cost function $J(\alpha)$ for all iterations using stochastic gradient descent method.*

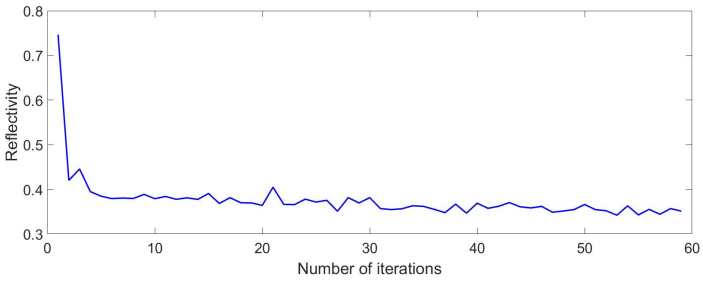


FIG. 5.3. *The cost function $J(\alpha)$ for all iterations using mini-batch stochastic gradient descent method.*

| optimal result(nm) | $\sigma_1(nm)$ | $\ell_1(nm)$ | $\sigma_2(nm)$ | $\ell_2(nm)$ | reflectivity |
|---|---|---|---|---|---|
| GD | 55 | 67 | 40 | 17 | 0.370 |
| SGD | 49 | 71 | 38 | 26 | 0.364 |
| mini-batch SGD | 44 | 65 | 45 | 24 | 0.368 |

TABLE 5.1. *The optimal parameters for Monte-Carlo method, stochastic gradient method and mini-batch SGD method.*

Table 5.1 shows that the results obtained form stochastic gradient method, mini-batch SGD method and gradient descent method are similar to each other, which is around 0.37. The reflectivity is diminished a lot compared to the reflectivity of the flat structure, which is 0.76 [19]. The gradient descent method is most stable in the three methods, however, the computational cost of the gradient descent method is much more than the other two methods. In the above example, we choose Monte-Carlo sample size $N = 1000$. The iteration stops after 7 steps, then we need to solve $1000 \cdot 7$ boundary value problems and the corresponding adjoint problems in Algorithm 1. When we employ the stochastic gradient method, only 1 sample needs to be calculated. It is required to solve 78 boundary value problems and the corresponding adjoint problems in Algorithm 2. In Algorithm 3, we choose the sample size $N_m = 20$. The computational cost for the mini-batch stochastic gradient descent method is to solve $59 \cdot 20$ boundary value problems and the corresponding adjoint problems.

The result of the reflectivity for all iterations by the mini-batch stochastic gradient descent method has less fluctuations compare to stochastic gradient method. For each iteration in the mini-batch stochastic gradient method, it is easy to accelerate the computation of the average gradient $\frac{1}{N_m}\sum_{i=1}^{N_m}\nabla R_\alpha(\omega_i)$ by using parallel computing skill. The mini-batch method is more stable and time efficient, so the mini-batch stochastic gradient descent method is the preferred method for our optimization problem.

**Example 2.** In this example, we consider the more challenging case when the incident wave has a larger wavelength. Since the incident wave has a larger wavelength, the reflectivity is relative larger and it is more difficult to find the optimal approach. We consider the case when the wave length is 720 nm. The refractive index of the absorbing layer is set as $4+0.0035i$ [18]. The refractive index of the TCO layer is 1.915, or equivalently, its relative permittivity $\varepsilon_{r,1} = 3.667$. The refractive index of the absorbing layer is $4+0.0035i$. The initial condition is chosen to be

$\alpha_1 = (\sigma_1, \ell_1) = (35nm, 20nm)$, $\alpha_2 = (\sigma_2, \ell_2) = (35nm, 20nm)$. We consider the normal incident case $\theta = 0$. The optimal results obtained from the gradient method, the stochastic gradient method and the mini-batch gradient method are shown in Figure 5.4 to Figure 5.6. The optimal parameters are listed in Table 5.2.

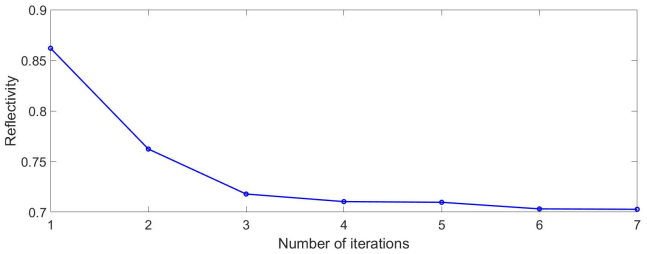


FIG. 5.4. *The cost function $J(\alpha)$ for all iterations using gradient descent method.*

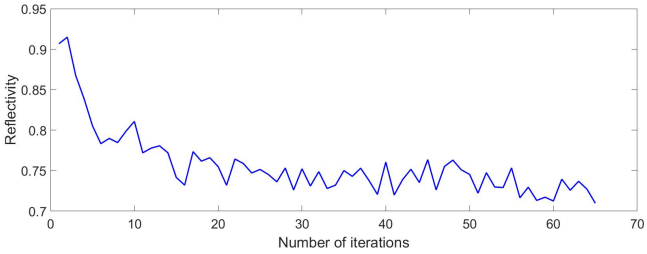


FIG. 5.5. *The cost function $J(\alpha)$ for all iterations using stochastic gradient descent method.*

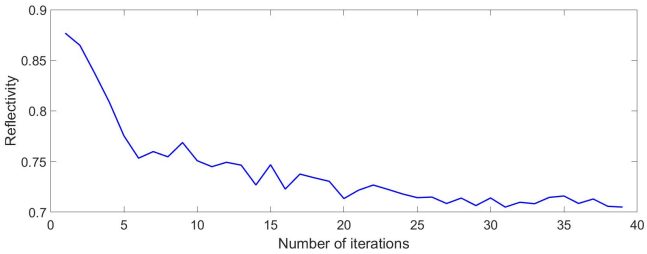


FIG. 5.6. *The cost function $J(\alpha)$ for all iterations using mini-batch stochastic gradient descent method.*

| optimal result(nm) | $\sigma_1(nm)$ | $\ell_1(nm)$ | $\sigma_2(nm)$ | $\ell_2(nm)$ | reflectivity |
|---|---|---|---|---|---|
| GD | 40 | 37 | 38 | 27 | 0.703 |
| SGD | 52 | 44 | 46 | 31 | 0.712 |
| mini-batch SGD | 49 | 38 | 50 | 32 | 0.705 |

TABLE 5.2. *The optimal parameters for Monte-Carlo method, stochastic gradient method and mini-batch SGD method.*

The reflectivities of the optimal structure obtained from the gradient descent method, stochastic gradient method and the mini-batch stochastic gradient method are around 0.7, in comparison, the reflectivity of the flat structure is 0.98 [19]. The mini-batch stochastic gradient method and the stochastic gradient method reduce the computational cost dramatically compared with the gradient descent method. In addition, the mini-batch stochastic gradient method is more stable than the stochastic gradient descent method. From the second example, we can see that the mini-batch gradient descent method is indeed a relatively stable method with less computational cost. It is reasonable to choose the mini-batch stochastic gradient method to get the optimal result for our problem.

## REFERENCES


[1] G. Bao and Y. Wang, *Optimal design of antireflection coatings with different metrics*, J. Opt. Soc. Am. A, 30:656–662, 2013. 1

[2] P. Bermel, C. Luo, L. Zeng, L.C. Kimerling, and J.D. Joannopoulos , *Improving thin-film crystalline silicon solar cell efficiencies with photonic crystals*, Opt. Exp., 15:16986–17000, 2007. 1

[3] A. Čampa, J. Krč, and M. Topič, *Analysis and optimisation of microcrystalline silicon solar cells with periodic sinusoidal textured interfaces by two-dimensional optical simulations*, J. Appl. Phys., 105:083107, 2009. 1

[4] J.C. Goldschmidt, M. Peters, A. Bösch, H. Helmers, F. Dimroth, S.W. Glunz, and G. Willeke, *Increasing the efficiency of fluorescent concentrator systems*, Sol. Energy Mat. Sol. Cells, 93:176–182, 2009. 1

[5] C. Rockstuhl and F. Lederer, *Photon management by metallic nanodiscs in thin film solar cells*, Appl. Phys. Lett., 94:213102, 2009. 1

[6] C. Battaglia, C.-M. Hsu, K. Söderström, J. Escarré, F.-J. Haug, M. Charrière, M. Boccard, M. Despeisse, D.T. L. Alexander, M. Cantoni, Y. Cui, and C. Ballif, *Light trapping in solar cells: can periodic beat random?* ACS Nano, 6:2790–2797, 2012. 1

[7] S. Fahr, C. Rockstuhl, and F. Lederer, *Engineering the randomness for enhanced absorption in solar cells*, Appl. Phys. Lett., 92:171114, 2008. 1, 5

[8] V.E. Ferry, M.A. Verschuuren, M. Claire van Lare, R.E.I. Schropp, H.A. Atwater, and A. Polman, *Optimized spatial correlations for broadband light trapping nanopatterns in high efficiency ultrathin film a-Si:H solar cells*, Nano Lett., 11:4239–4245, 2011. 1

[9] P. Kowalczewski, M. Liscidini, and L. Andreani, *Engineering Gaussian disorder at rough interfaces for light trapping in thin-film solar cells*, Opt. Lett., 37:4868–4870, 2012. 1, 5

[10] C. Rockstuhl, S. Fahr, K. Bittkau, T. Beckers, R. Carius, F.-J. Haug, T. Söderström, C. Ballif, and F. Lederer, *Comparison and optimization of randomly textured surfaces in thin-film solar cells*, Opt. Exp., 18:A335–A342, 2010. 1, 5

[11] J. Müller, R. Bernd, J. Springer, and M. Vanecek, *TCO and light trapping in silicon thin film solar cells*, Sol. Energy, 77:917–930, 2004. 1

[12] S. Vaswani, A. Mishkin, I. Laradji, M. Schmidt, G. Gidel, and S. Lacoste-Julien, *Painless stochastic gradient: interpolation, line-search, and convergence rates*, Adv. Neural. Inf. Process. Syst., 32:3732–3745, 2019. 1

[13] G. Bao, Y. Lin, and X. Xu, *Inverse scattering by a random periodic structure*, SIAM J. Numer. Anal., 58(5):2934–2952, 2020. 2.2

[14] G. Bao and P. Li, *Maxwell's Equations in Periodic Structures*, Springer, Beijing, 2021. 2.1

[15] H. Robbins and S. Monro, *A stochastic approximation method*, Ann. Math. Statist., 22(3):400–407, 1951. 4.3

[16] J. Kiefer and J. Wolfowitz, *Stochastic estimation of the maximum of a regression function*, Ann. Math. Statist., 23(3):462–466, 1952. 4.3

[17] B. Léon, F.E. Curtis, and N. Jorge, *Optimization methods for large-scale machine learning*, SIAM. Rev., 60:223–311, 2018. 4.3

[18] M. Zeman, R.A.C.M.M. van Swaaij, and J.W. Metselaar , *Optical modeling of a-Si:H solar cells with rough interfaces: Effect of back contact and interface roughness*, J. Appl. Phys., 88:6436–6443, 2000. 5, 5

[19] G. Bao, Y. Cao, J. Lin, and H.W. Van Wyk, *Computational optimal design of random rough surfaces in thin-film solar cells*, Commun. Comput. Phys., 25(5):1591–1612, 2019. 2.1, 5, 5